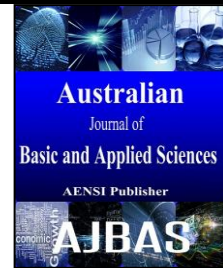




ISSN:1991-8178

## Australian Journal of Basic and Applied Sciences

Journal home page: www.ajbasweb.com



### High Efficiency Photovoltaic Grid-Tied-Interleaved Fly back Micro Inverter Using Optimal Control Method

<sup>1</sup>S. Sakthivel and <sup>2</sup>A.Ruby Meena

<sup>1</sup>PG Scholar Department of EEE Government College of Engineering Salem, India

<sup>2</sup>Assistant professor, Department of EEE Government College of Engineering Salem, India

#### ARTICLE INFO

##### Article history:

Article Received : 12 January 2015

Revised: 1 May 2015

Accepted: 8 May 2015

##### Keywords:

AC module, grid-connected, interleaved flyback,microinverter, photovoltaic (PV).

#### ABSTRACT

This project “High Efficiency Photovoltaic Grid-Tied-Interleaved Flyback Microinverter using Optimal Control Method” is composed of an Boundary conduction mode (BCM) and discontinuous conduction mode (DCM) control strategies which are widely used in the flyback microinverter. The BCM and DCM control strategies are investigated for the interleaved flyback microinverter concentrating on the loss analysis under different load conditions. These two control strategies have different impact on the loss distribution and thus the efficiency of the flyback microinverter. For the interleaved flyback microinverter, the dominant losses with heavy load include the conduction loss of the power MOSFETs and diodes, and the loss of the transformer; while the dominant losses with light load include the gate driving loss, the turn-off loss of the power MOSFETs and the transformer core loss. Based on the loss analysis, a new hybrid control strategy combining the two-phase DCM and one-phase DCM control is proposed to improve the efficiency in wide load range by reducing the dominant losses depending on the load current.

© 2015 AENSI Publisher All rights reserved.

**To Cite This Article:** S. Sakthivel and A. Ruby Meena., High Efficiency Photovoltaic Grid-Tied-Interleaved Fly back Micro Inverter Using Optimal Control Method. *Aust. J. Basic & Appl. Sci.*, 9(21): 14-22, 2015

#### INTRODUCTION

The interest in exploring renewable energies has grown in the last years due to the energy crisis. Photovoltaic (PV) sources are predicted to have the highest increase 30% in the next decade and to be the biggest contributor on the electricity generation. A PV ac module, which is also called the microinverter, is becoming more and more popular and the power range is normally up to about 200 W.

Compared to the conventional centralized, string and multistring inverter, the microinverter has many advantages such as higher maximum power point tracking (MPPT) efficiency and lower manufacturing cost through mass production, as well as safe and simple installation. With the rapid development of the market, a lot of research work has been done with the topologies and control methods of the microinverters. Normally, a boost stage is used to boost the low voltage source provided by the PV panel. An ac module based on dc bus was presented. A modulated boost stage is used to generate a rectified sinusoidal waveform and a current source inverter (CSI) is used to unfold the rectified waveform into the grid. These topologies usually achieve high efficiency under heavy load, but low efficiency under light load (no

more than 90% as reported). Moreover, the complexity and additional components of the previous topologies also result in high cost and low power density as a PV ac module. Alternatively, the microinverter derived from the flyback converter, named as the flyback inverter, is widely used due to its simple structure, lower cost, and higher efficiency.

A flyback dc/dc converter with high frequency isolation along with a H-Bridge pulse width modulation (PWM) inverter offers a simple two-stage approach. A high dc bus voltage allows for the low decoupling capacitance. But both stages operate at high frequency, the total losses are relatively high. A single-stage flyback inverter with the center-tapped secondary winding was presented. Each of the secondary winding transfers the energy to the ac side during a half-line period with two additional MOSFETs. A modulated flyback dc/dc converter followed by a CSI was presented.

The SCRs are used in the unfolding stage to reduce the cost and conduction loss. To further improve the efficiency, a soft-switching-interleaved flyback microinverter under boundary conduction mode (BCM) was presented. Active clamp and synchronous rectifier technology were adopted. But

additional auxiliary circuit components are required and this results in higher cost, lower power density, and complex control as a PV ac module. A multiphase-interleaved flyback microinverter with the hybrid control scheme including the interleaved mode and quasiresonant mode is proposed by Emphas Technology.

But either a simple flyback mode or an interleaved flyback mode is applied during a half-line period depending on the output power of the PV panel, which limits the further improvement of the efficiency. A dual-mode switching strategy for the center-tapped secondary winding flyback inverter was presented.

The BCM and discontinuous conduction mode (DCM) modulations were used simultaneously during a half-line period, because BCM is more suitable to high-power levels and DCM is better for low-power levels as far as the efficiency is concerned. Owing to the combined control strategy, higher efficiency can be achieved over the conventional BCM control method without additional cost. The reference signal design with the similar control strategy for the single flyback converter with a CSI was proposed.

However, the optimal boundary point between the BCM and DCM are applied to is not clarified regarding to the interleaved microinverters. The two phase inverters are modulated with the same control strategy during the half-line period, and this limits the efficiency improvement within wide load condition. More importantly, the boundary condition of the hybrid control with BCM and DCM is not analyzed, which is so important to design the power stage and the controller for the optimization of the overall performance.

In this paper, the BCM and DCM control strategies are investigated of the interleaved fly back microinverter concentrating on the loss analysis under different load conditions, respectively. It is noted that the DCM control strategy achieves higher efficiency over BCM for the application of the interleaved fly back micro inverter within the power range of 200W.

The advantages of two-phase DCM operation are the current sharing and the reduction of the current stress between two interleaved phases so that the conduction loss and turn-off loss of the power MOSFETs and diodes as well as the copper loss of the transformer can be reduced with higher output power. On the other hand, the advantage of one-phase DCM operation is the reduction of the transformer core loss, the driving loss of the power MOSFETs with lower output power. Since the output power is a pulsating power following a squared sine wave, the idea here is to combine two-phase DCM modulation and one-phase DCM modulation simultaneously according to different output power during a half-line period. So that the dominant

losses can be optimized and high efficiency is achieved in wide load range.

In addition, the proposed control method is compatible with the digital implementation and requires no additional auxiliary circuitry. Section II presents the analysis of the interleaved flyback microinverter under BCM and DCM. Section III presents the proposed control method and its principle of operation. Section IV presents the hardware and software design. The simulation results are also provided in Section V. Section VI contains the experimental results and discussion. Section VII provides a brief conclusion.

### ***Analysis Of Flyback Inverter Under Bcm And Dcm:***

#### ***A. Topology of the Interleaved Flyback Microinverter:***

Fig. 1 shows the main circuit of the interleaved flyback inverter. The inverter comprises of two-phase-interleaved flyback converters and a CSI. S1 and S6 are the main power switches; D1 and D2 are the rectifier diodes; NP 1 and NP 2 are the primary windings, and NS1 and NS2 are the secondary windings. S3–S6 form the CSI to unfold the rectified sinusoidal waveform into the grid. S3 and S6 turn ON during the positive-half grid period, while S4 and S5 turn ON during the negative-half grid period. Fig. 2 shows the current waveforms of the interleaved flyback inverter.

Each phase is 180° phase shifted in one switching period to achieve ripple cancellation. Thus, a lower output filter inductance can be used.

#### ***B. Comparison of BCM and DCM:***

Fig. 3 shows key waveforms of the interleaved flyback microinverter under BCM and DCM, respectively. Under DCM, a constant switching frequency control is applied. A variable switching frequency is applied under BCM to achieve sinusoidal output current waveform. It is noticed that the output current frequency is twice of the switching frequency, which leads to the output filter inductance reduction and higher power density can be achieved.

The dominant losses with heavy load include the conduction loss of the MOSFETs and diodes, and the core loss and copper loss of the transformer, while the dominant losses with light load include the driving loss, turn-off loss of the MOSFETs and the transformer core loss. The range of the switching frequency increases dramatically as the power level decreases for the flyback microinverter under BCM.

For the microinverter with two phases, the switching frequency range varies from 113 to 480 KHZ under BCM at the power level of 200 W. This causes the driving loss and turn-off of the MOSFETs to increase significantly. Therefore, the efficiency under BCM is much lower than DCM under the light-load condition. Table I shows the loss distribution comparison under BCM and DCM under the halfload condition. The specifications are as follows: input

voltage:  $V_{dc} = 36\text{--}60\text{ V}$ ; grid voltage:  $V_g = 220\text{ VAC}$ ; grid frequency:  $f_{grid} = 50\text{ Hz}$ ; switching frequency:  $f_s = 100\text{ kHz}$ .

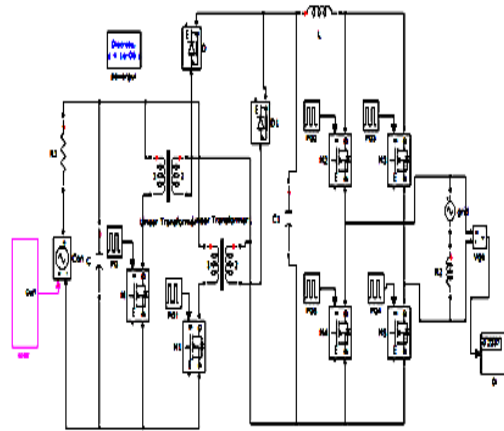


Fig. 1: Interleaved flyback inverter.

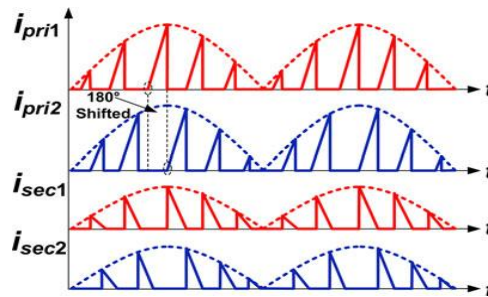


Fig. 2: Current waveforms of the interleaved flyback inverter.

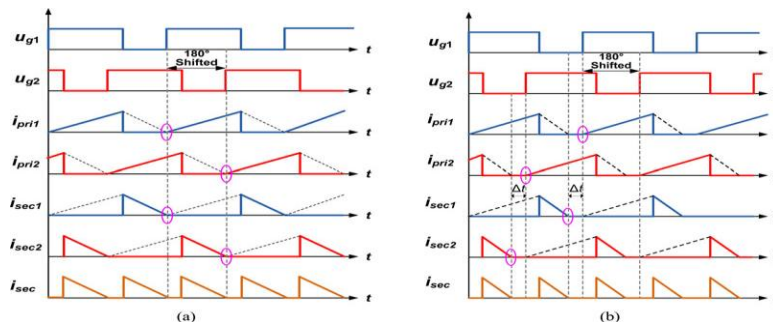


Fig. 3: Key waveforms of the interleaved flyback inverter under BCM and DCM. (a) BCM. (b) DCM.

Table I: Estimated Loss Distribution Under Bcm And Dc Forthemicroinverter With Two-Phase Operation.

	DCM		BCM	
	Loss	Percentage	Loss	Percentage
$P_{off}$	0.80 W	18.3%	2.50 W	31.5%
$P_{drive}$	0.83 W	18.9%	2.83 W	35.7%
$P_{mos}$	0.60 W	13.7%	0.40 W	5.04%
$P_{core}$	0.84 W	19.2%	0.99 W	12.5%
$P_{cu}$	0.71 W	16.2%	0.89 W	11.2%
$P_{diode}$	0.60 W	13.7%	0.32 W	4.04%

The components of the power train are as follows: the transformer:  $L_p = 28 \mu\text{H}$ ,  $L_s = 112 \mu\text{H}$ ; S1 and S2 : SPW52N50C3(560 V/52 A from Infineon); D1 and D2 : IDP12E120(1200 V/12 A from Infineon); S3–S6 : S8016N (800 V/16 A from Teccor). The detailed design procedure is provided in Section IV.

In this paper, the loss analysis is based on the previous specifications. Fig. 4 shows the calculated efficiency of the interleaved flyback microinverter under DCM and BCM, respectively. It is noted that the turn-off loss  $P_{off}$  and the gate driving loss  $P_{drive}$  under BCM are much higher than DCM.

This translates into a significant reduction of the light load efficiency. A comparison of the microinverter under BCM and DCM is shown in Table II. Based on the previous analysis, it should be

pointed that for the application of the interleaved flyback microinverter, within the power range of 200 W, DCM has the advantage over BCM. However, it should be noted that even under DCM, the microinverter suffers low efficiency when the load current reduces.

Since the peak current control is used under BCM, both primary and secondary current of the transformer need to be sensed. While for the DCM control, the current programmed control is used and only the output current is sensed. The total harmonic distortion (THD) of the DCM operation is 3.79% as illustrated. Due to the large frequency bandwidth, BCM achieves lower THD as 2.45%. The proposed control only uses the DCM modulation, the THD of the output current will meet the industrial requirement (<5%) such as IEC 61727.

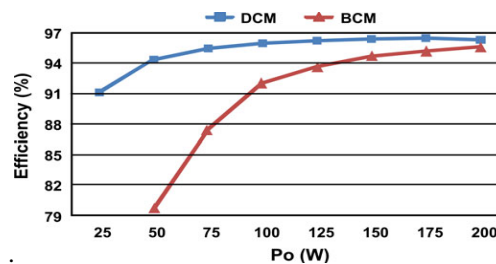


Fig. 4: Calculated efficiency comparison under DCM and BCM for the microinverter with two phase.

Table II: Comparison Of Bcm And Dcm.

	BCM	DCM
Switching frequency	VSF	CSF
Power transfer	High	Low
Peak current sensing	Yes	No
Control	Complex	Easy
THD	Low	High
Loss under light load	High	Low

Table III: Estimated loss distribution of DCM under different load conditions for the microinverter with two-phase operation.

	Full load		Quarter load	
	Loss	Percentage	Loss	Percentage
$P_{off}$	1.32 W	16.8%	0.60 W	18.2%
$P_{drive}$	0.83 W	10.5%	0.83 W	25.2%
$P_{mos}$	1.70 W	21.6%	0.22 W	6.7%
$P_{core}$	1.48 W	18.8%	1.08 W	32.7%
$P_{cu}$	1.22 W	15.5%	0.27 W	8.1%
$P_{diode}$	1.32 W	16.8%	0.30 W	9.1%

### III. Proposed Control Method And Principle of Operation:

#### A. Loss Analysis of DCM:

Table III shows the calculated loss distribution of a 200-W-interleaved fly back inverter under 100% and 25% load, respectively. It is observed that the dominant losses with heavy load include the

conduction loss of the power MOSFETs,  $P_{mos}$  and diodes  $P_{diode}$ , the transformer core loss  $P_{core}$  and copper loss  $P_{cu}$ , whereas the dominant losses with light load include the gate driving loss  $P_{drive}$ , the turn-off loss  $P_{off}$  of the power MOSFETs and the transformer core loss  $P_{core}$ .

Therefore, minimizing the dominant losses according to load condition is an effective way to optimize the efficiency in wide load range. For simplicity, 1 $\Phi$  DCM represents only one phase operation and 2 $\Phi$  DCM represents two phases operation under the interleaved mode. On the one hand, the 2 $\Phi$  DCM operation shares the current and reduces the current stress between two interleaved phases.

This is beneficial to reduce the conduction loss and turn-off loss of the power MOSFETs and diodes, as well as the copper loss of the transformer under the heavy-load condition. On the other hand, the 1 $\Phi$  DCM operation sheds the additional phase of the microinverter, which minimizes the gate driving loss of the power MOSFETs as well as the core loss of the transformer under the light-load condition.

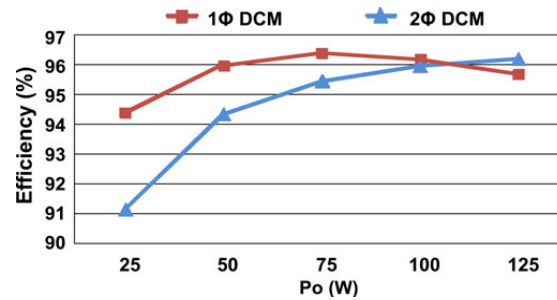


Fig. 5: Calculated efficiency of the interleaved fly back inverter.

Based on the loss analysis, Fig. 5 shows the efficiency of the interleaved fly back inverter under 1 $\Phi$  DCM and 2 $\Phi$  DCM operation. For the sake of the output power, the maximum power transferred by

each phase is about 125W under DCM operation. It is noted that the efficiency improves while operating under 1 $\Phi$  DCM within the power range of 105 W.

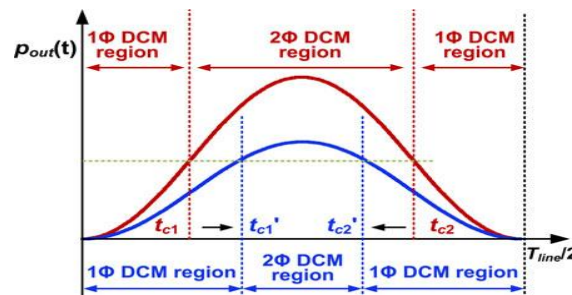


Fig. 6: Output power curve with 1 $\Phi$  DCM and 2 $\Phi$  DCM for the interleaved flyback microinverter. Actually, 2 $\Phi$  DCM and 1 $\Phi$  DCM can be used simultaneously to modulate the interleaved flyback inverter depending on the load current during a half-line period.

### B. Proposed Hybrid Control Method:

From the previous analysis, it is interesting to notice that the advantage of 2 $\Phi$  DCM operation is current sharing between two phases. The conduction loss and turn-off loss of the power MOSFETs and diodes and the copper loss of the transformer can be reduced when the load current is high. The 1 $\Phi$  DCM operation reduces the driving loss of the power MOSFETs and the transformer core loss. The conventional DCM control only shuts down one phase when the load reduces to some power level. Actually, during the half-line period, either 2 $\Phi$  DCM or 1 $\Phi$  DCM control can be applied.

It is noticed that the output power  $p_{out}(t)$  during a half-line period is a pulsating power following a squared sine wave:  $P_{out}(t) = 2P_o \sin^2(\omega t)$  (1) where  $P_o$  presents the average value of the output power delivered to the grid.

The idea here is to combine the advantages of 2 $\Phi$  DCM and 1 $\Phi$  DCM adaptively to the load current during which is similar to the phase shedding technology so that the efficiency can be optimized in wide load range. Fig. 6 shows the operating region of 1 $\Phi$  DCM and 2 $\Phi$  DCM during a half-line period.

In Fig. 6, 2 $\Phi$  DCM is employed when load current is high and 1 $\Phi$  DCM is employed when the load current is under a certain level. In this way, the dominant losses are reduced depending on the load current and higher efficiency can be achieved in wide load range. Moreover, the proposed control is compatible with the digital implementation without additional cost.

It should be noted that as  $P_o$  decreases, the 2 $\Phi$  DCM region decreases simultaneously. In particular, when  $P_o$  decreases to a certain level, the hybrid modulation merges into only 1 $\Phi$  DCM. In

additional, it should be noted that 2Φ DCM and 1Φ DCM modulations operate simultaneously during a

half-line period since the proposed control is based on the instantaneous power delivered to the grid.

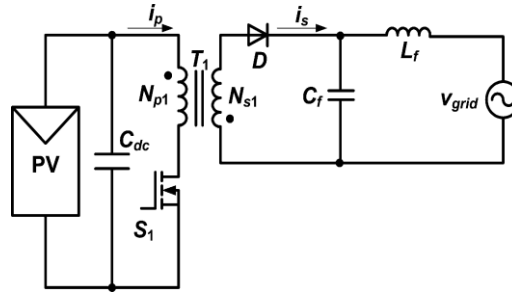


Fig. 7: Equivalent circuit of a single-phase flyback inverter.

### C. Analysis and Design of Reference Signal for the Proposed Control:

For the proposed control method, the reference signal  $i_{ref}$  is used to generate the modulated duty cycles and needs to be well designed so that high efficiency and low THD can be achieved. Since the equivalent circuits of the two modules are similar, DCM of a single-phase flyback inverter is analyzed first. Fig. 7 shows the equivalent circuit of the single flyback inverter during a half-line period.

During the S1 ON time, the primary current  $i_p$  increases gradually in a linear relationship with the input voltage  $V_{dc}$  and the primary inductance  $L_p$ . During the S1 OFF time, the second current is decreases in a linear relationship with the grid voltage  $v_g(t)$  and the secondary inductance  $L_s$ . The turn-on time  $T_{on}$  and turn-off time  $T_{off}$  in every switching period are where  $I_p$  and  $I_s$  are the peak value of  $i_p$  and  $i_s$  in each switching period, respectively. Since  $I_p$  equals the reference signal  $i_{ref}$ , the relationships of  $I_p$  and  $I_s$  are.

$$T_{on} = \frac{L_p \cdot I_p}{V_{dc}} \quad (2)$$

$$T_{off} = \frac{L_s \cdot I_s}{v_g(t)} \quad (3)$$

$$I_p = i_{ref} \quad (4)$$

$$I_s = I_p \cdot \sqrt{\frac{L_p}{L_s}} = i_{ref} \cdot \sqrt{\frac{L_p}{L_s}} \quad (5)$$

There is an approximation relationship as (6), where the RMS value of the output current  $i_{out}$  equals the average value of  $i_s$  in every switching period.

### Design Procedure And Implementation:

#### A. Design Example:

Based on the previous analysis, the interleaved flyback inverter of 200 W is presented as a design example and verifies the proposed hybrid control method. The specifications are as follows: input

voltage [maximum power point (MPP)]:  $V_{dc} = 50$  V; grid voltage: 220 VAC; grid frequency:  $f_{grid} = 50$  Hz; switching frequency:  $f_s = 100$  kHz; transformer turns ratio:  $n = N_p/N_s = 0.5$ . It should be mentioned that the turns ratio has a close relationship with the voltage and current stress of each component.

#### B. Realization of MPPT:

The PV array under uniform irradiance exhibits a current-voltage characteristic with a unique point, called the MPPT, here the array produces maximum output power. Fig. 8(a) shows an example of the PV module characteristics in terms of the PV output current versus the voltage. Fig. 8(b) shows the output power versus the current for different irradiance levels  $G$ .

As noted in Fig. 8, since the  $I - V$  characteristic of the PV array, and hence its MPP, changes as a consequence of the variation of the irradiance level, it is necessary to track continuously the MPPT in order to maximize the power output from a PV system as far as the PV system efficiency is concerned. There are many different control algorithms that have been proposed to realize the MPPT, such as the perturb and observe (P&O), the incremental conductance, the fuzzy logic and the neural network, etc. concerned.

In this paper, the P&O technique is used owing to its simple implementation and low cost.

#### C. Design of the Input Capacitance:

For the single-stage grid-connected microinverter, the MPPT provides the constant output power from the PV panel  $P_{pv}$ , while the power transferred to the grid  $p_{out}(t)$  is a pulsating waveform as shown in (1). Generally, the electrolytic capacitor is used to measure the unbalance of the input and output power.

When  $P_{pv}$  is surplus to  $p_{out}(t)$ , the reminded power is stored into the decoupling capacitor. On the contrary, when  $P_{pv}$  is smaller than  $p_{out}(t)$ , the decoupling capacitor delivers the power to the output.

The input and output waveforms are shown in Fig. 9. The value of the decoupling capacitor is

determined by the energy that has to be stored in the capacitor, whose size is

$$C_{dc} = \frac{P_{pv}}{\omega V_{dc} \Delta V} \tag{23}$$

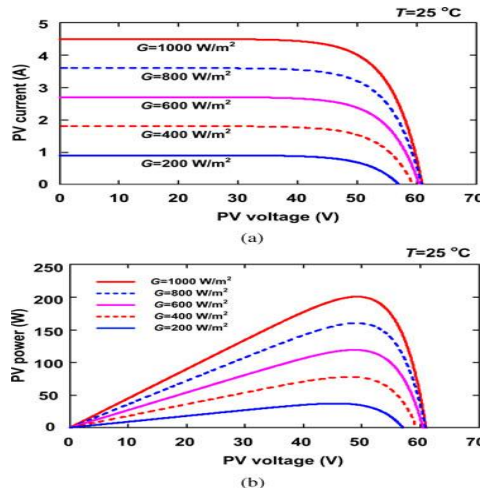


**Fig. 8:** PV module characteristics for different irradiance levels G. (a) Output current versus voltage. (b) Output power versus voltage.

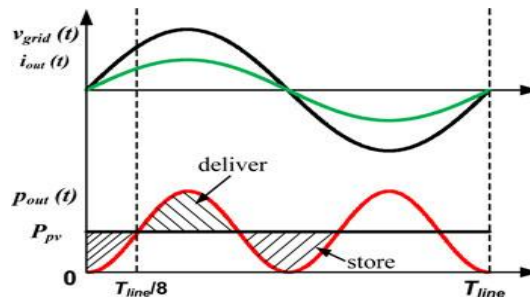


**Fig. 9:** Input and output waveforms.

where  $\omega$  is the angle frequency of the grid voltage, and  $\Delta V$  is the maximum peak-to-peak ripple voltage of the input capacitor. For  $P_{pv} = 200$  W,  $\omega = 2\pi f = 100\pi$ ,  $V_{dc} = 50$  V, and  $\Delta V = 2$  V, the required input capacitance is  $C_{dc} = 6.37$  mF. Four 1.8-mF electrolytic capacitors are paralleled with lower ESR.

**D. Software Design:**

Fig. 10. shows the control block diagram of the interleaved flyback inverter with the proposed control. The control blocks are implemented by Freescale DSP MC56F8257. In Fig. 10, phase-locked loop is used to detect the phase angle, amplitude, and frequency of the grid voltage. An MPPT block is used to track the MPP of the PV panel.

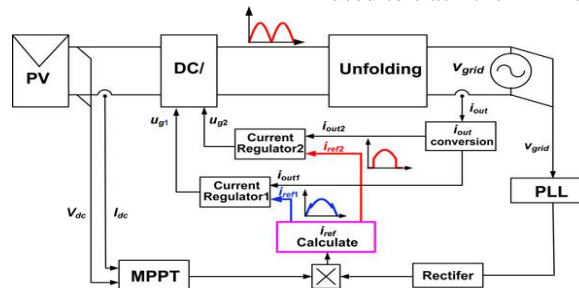


**Fig. 10:** Control diagram of an interleaved flyback microinverter.

In the ADC interrupt,  $V_{dc}$ ,  $I_{dc}$ ,  $V_{grid}$ , and  $I_{out}$  are sampled. The conversion results are used to achieve the zero-crossing detecting and calculate the input power  $P_{pv}$ . Timer 1 is used to generate a 20 kHz periodic interrupt, in which the reference signal

$i_{ref1}$  and  $i_{ref2}$  can be calculated. Then,  $i_{ref1}$  and  $i_{ref2}$  are sent to the PWM reload interrupt in order to calculate the duty cycle of each phase.

**Simulation Results And Discussion:**

A simulation model of the proposed control has been developed.

The specifications of the interleaved flyback microinverter are as follows: input voltage  $V_{dc} = 36-60V$ ; Grid voltage  $V_{grid} = 220V$ ; grid frequency:

$f_{grid} = 50\text{ Hz}$ ; switching frequency  $f_s = 100\text{ kHz}$ ; Gate drive voltage  $V_g = 15$ ; primary inductance:  $L_P = 28\ \mu\text{H}$ , and the turns ratio  $n = 0$ .

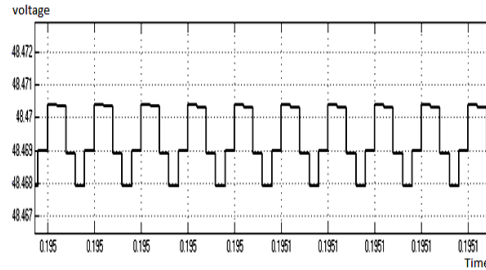


**Fig. 11:** Input voltage waveform

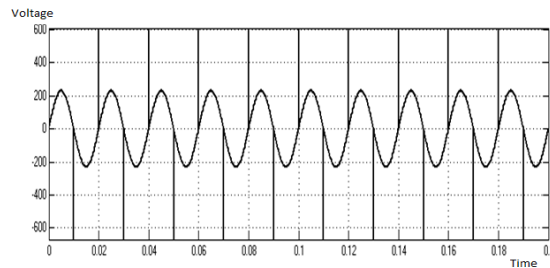


**Fig. 12:** Output voltage waveform.

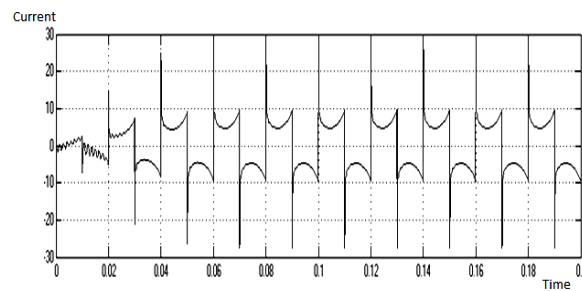


**Fig. 13:** Output current waveform.

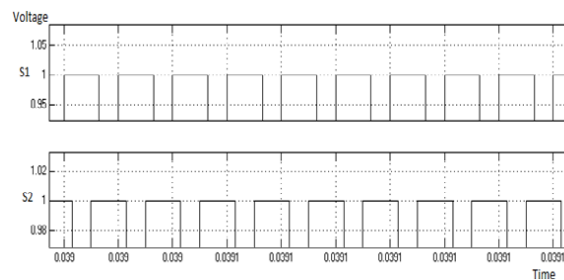


**Fig. 14:** Inverter Switching Frequency.

**Experimental Results and Discussion:**

To verify the proposed hybrid control method, a prototype of 200 W has been built. The specifications are the same as the analysis in Section V. A PV array simulator is used to verify the MPPT function of the proposed control.

The major components used in the circuit are listed as follows:  $S1$  and  $S2$  SPW52N50C3;  $D1$  and  $D2$  : IDP12E120;  $S3-S6$  : S8016N; the transformer: RM12,  $L_P = 28\ \mu\text{H}$ ,  $L_s = 112\ \mu\text{H}$ ,  $L_k = 0.55\ \mu\text{H}$ ; the output filter inductance:  $L_f = 600\ \mu\text{H}$ ; the output filter capacitor:  $C_f = 0.33\ \mu\text{F}$ .

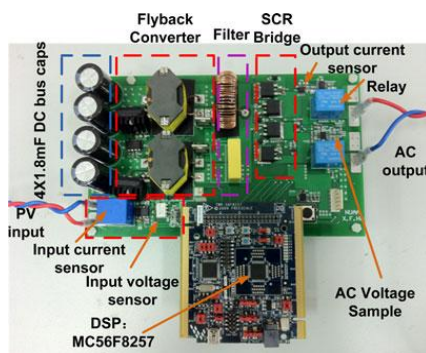


**Fig. 15:** Photograph of a prototype.

The photograph of a prototype is illustrated in Fig. 15.

A hall effect sensor BJHCS-PS5 is used to sample the input current and an isolation amplifier HCPL-7840 is used to sample the input voltage.

Therefore, the input power can be obtained. A hall effect-based linear current sensor IC ACS712ELCTR-05B-T is used to sense the output current. Two relays are used to achieve grid connection. A Freescale DSP MC56F8257 demo board is used to implement the proposed hybrid control.

#### **Conclusion:**

This project has presented Photovoltaic Grid-Tied-Interleaved Flyback Microinverters to Achieve High Efficiency in Wide Load Range. Simulation results are obtained, showing a good agreement with the theoretical analysis. The loss distribution and the efficiency of the interleaved flyback microinverter under BCM and DCM are investigated analytically under different power levels. It is found that DCM is a better choice than BCM within the power range of 200 W. For the interleaved flyback microinverter, the dominant losses with heavy load include the conduction loss of the power MOSFETs and diodes, the core loss and copper loss of the transformer, while the dominant losses with light load include the gate driving loss, turn-off loss of the power MOSFETs and the transformer core loss. The 2 $\Phi$  DCM operation shares the current and reduces the current stress between two interleaved phases. The conduction loss and turn-off loss of the power MOSFETs and diodes and the copper loss of the transformer can be reduced at heavy load, and the 1 $\Phi$  DCM reduces the driving loss of the main MOSFETs and the core loss of the transformer under the light-load condition. A new hybrid control strategy combining the 2 $\Phi$  DCM and 1 $\Phi$  DCM control during a half-line period is proposed. With the proposed control strategy, high efficiency can be achieved in wide load range by reducing the dominant losses depending on the load current.

#### **REFERENCES**

- Zhiliang Zhang, Member, IEEE, Xiao-Fei He and Yan-Fei Liu, 2013. Fellow, IEEE Transactions on power electronics, 28-11.
- Yu, W., C. Hutchens, J.S. Lai and T. Hegarty, 2009. "High efficiency converter with charge pump and coupled inductor for wide input photovoltaic AC module application," in Proc. IEEE Energy Convers. Congr. Expo., 3895–3900.
- Kjaer, S.B., J.K. Pedersen and F. Blaabjerg, 2005. "A review of single-phase grid-connected inverter for photovoltaic modules," IEEE Trans. Ind. Appl., 41(5): 1292–1306.
- Li, Q. and P. Wolfs, 2008. "A review of the single phase photovoltaic module integrated converter topologies with three different DC link configurations," IEEE Trans. Power Electron., 23(3): 1320–1333.
- Zhang, L., K. Sun, Y. Xing, L. Feng, and H. Ge, 2011. "A modular grid-connected photovoltaic generation system based on DC bus," IEEE Trans. Power Electron., 26(2): 523–531.
- Jiang, S., D. Cao, Y. Li and F.Z. Peng, 2012. "Grid-connected boost-half-bridge photovoltaic microinverter system using repetitive current control and maximum power point tracking," IEEE Trans. Power Electron., 27(11): 4711–4722.
- Liang, Z., R. Guo, J. Li and A.Q. Huang, 2011. "A high-efficiency PV module integrated DC/DC converter for PV energy harvest in FREEDM system," IEEE Trans. Power Electron., 26(3): 897–909.
- Prapanavarat, C., M. Barnes and N. Jenkins, 2002. "Investigation of the performance of a photovoltaic AC module," IEE Proc. Gener., Trans. Distrib., 149(4): 472–478.
- Shimizu, T. and S. Suzuki, 2011. "Control of a high efficiency PV inverter with power decoupling function," in Proc. IEEE Int. Conf. Power Electron. ECCE Asia, 1533–1539.
- Kutkut, N. and H. Hu, 2010. "Photovoltaic micro-inverter: Topologies, control aspects, reliability issues, and applicable standards," in Proc. IEEE Energy Convers. Congr. Expo., 5–18.